Available online at www.sciencedirect.com
ScienceDirect
Journal of Nuclear Materials 366 (2007) 369–387
journal of nuclear materials
www.elsevier.com/locate/jnucmat

# Microstructural and mechanical property changes with aging of Mo–41Re and Mo–47.5Re alloys

Keith J. Leonard *, Jeremy T. Busby, Steven J. Zinkle

*Materials Science and Technology Division, Oak Ridge National Laboratory, Oak Ridge, TN 37831, United States*

**Abstract**

The changes in microstructure and mechanical properties of Mo–41Re and Mo–47.5Re alloys were investigated following 1100 h thermal aging at 1098, 1248 and 1398 K. The electrical resistivity, hardness and tensile properties of the alloys were measured both before and after aging, along with the alloy microstructures though investigation by optical and electron microscopy techniques. The Mo–41Re alloy retained a single-phase solid solution microstructure following 1100 h aging at all temperatures, exhibiting no signs of precipitation, despite measurable changes in resistivity and hardness in the 1098 K aged material. Annealing Mo–47.5Re for 1 h at 1773 K resulted in a two-phase $\alpha$Mo + $\sigma$ structure, with subsequent aging at 1398 K producing a further precipitation of the $\sigma$ phase along the grain boundaries. This resulted in increases in resistivity, hardness and tensile strength with a corresponding reduction in ductility. Aging Mo–47.5Re at 1098 and 1248 K led to the development of the $\chi$ phase along grain boundaries, resulting in decreased resistivity and increased hardness and tensile strength while showing no loss in ductility relative to the as-annealed material.
Published by Elsevier B.V.

*PACS:* 81.40.Cd; 81.05.Bx; 89.30.Gg; 62.20.Fe

## 1. Introduction

Molybdenum-base alloys have attracted considerable interest for use as structural materials for applications in the energy and aerospace fields due to their high temperature strength, high thermal conductivity and corrosion resistance. As a means to improve ductility, toughness and fabricability, the addition of Re to Mo has long been recognized [1–6]. This 'rhenium effect' is observed when Group VIa metals are alloyed with elements from Group VIIa and VIIIa metals [7,8]. However differing explanations exist on the cause of this effect, ranging from enhancement of mechanical twinning, solid solution softening through decreased resistance to dislocation glide, reduction of oxygen content at grain boundaries and increased interstitial oxygen solubility [2,5,6,9–12].

Dilute Mo–Re alloys (<18 wt% Re) have been previously reported to have maximum tensile ductility at 11–13 wt% Re in room temperature tests [13,14]. However, in a subsequent critical review of the data, Wadsworth et al. [15,16] found that many of these claims were not conclusive due to inadequately controlled C and O impurity levels. As a result, the improved performance of Mo–Re with

* Corresponding author. Fax: +1 865 241 3650.
*E-mail address:* leonardk@ornl.gov (K.J. Leonard).

0022-3115/$ - see front matter Published by Elsevier B.V.
doi:10.1016/j.jnucmat.2007.03.027

Re contents from 10 to 30 wt% Re alloys is largely unproven. However, more concentrated Mo–Re alloys (with 40–50 wt% Re) are used extensively in industries ranging from medicine to defense. In particular, two alloys (with 41 and 47.5 wt% Re) have been commercially available since the 1960s. These alloys are more expensive and dense than unalloyed Mo, but possess better ductility, mechanical properties, thermal properties, and fabricability.

Alloys with Re concentrations up to 41 wt% consist of single-phase solid solution alloys, with higher Re concentrations developing second phase structures. However, some disagreement exists on the actual solubility limit for Re especially at low temperature where diffusion kinetics are particularly slow. Two commercially available Mo–Re alloys of interest to space reactor applications incorporate these two alloy designs with Re concentrations of 41 and 47.5, with the later frequently termed as 'Mo–50Re'.

Recently, Mo–Re alloys have become of interest as candidate materials for fission space reactor designs. Preliminary mechanical property data on Mo–41Re and Mo–47.5Re alloys has been limited to tests conducted on material annealed at various temperatures. Only a limited database exists on the phase development associated with lower temperature aging of these alloys, with much of this work reported for ion and neutron irradiated materials. The objective of this work is to investigate the microstructural changes occurring in Mo–41Re and Mo–47.5Re alloys following 1100 h aging at space reactor relevant temperatures and the impact of aging on the mechanical properties. The changes in electrical resistivity, hardness and tensile properties were compared to that of the as-annealed condition.

## 2. Experimental

### 2.1. Sample fabrication

The Mo–41Re alloy examined in this study was produced at the Oak Ridge National Laboratory (ORNL), heat number MR1, through vacuum arc re-melting. The Mo–47.5Re alloy was provided by Pittsburgh Materials Technology Inc. (PMTI), heat number CVAM1571. The measured alloy compositions in the as-received condition and following thermal anneal and aging conditions are presented in Table 1. Chemical analysis of the annealed and aged materials was provided by Wah Chang, while analysis of the as-received Mo–47.5Re was performed by PMTI. Analysis of the Re concentration

Table 1
Actual compositions of the alloys in the as-received condition and following heat treatment

| Element | Mo–41Re | | | | | Mo–47.5Re | | | | |
|---|---|---|---|---|---|---|---|---|---|---|
| | As-received | 1773 K Anneal | 1098 K Aged | 1248 K Aged | 1398 K Aged | As-received | 1773 K Anneal | 1098 K Aged | 1248 K Aged | 1398 K Aged |
| Mo (wt%) | Bal. | 58.09 | 58.01 | 59.33 | 59.15 | Bal. | 52.81 | 52.75 | 52.75 | 53.18 |
| Re (wt%) | 40.1 | 41.90 | 41.98 | 40.66 | 40.84 | 46.8 | 47.18 | 47.24 | 47.24 | 46.81 |
| *Interstitial impurities (wppm)* | | | | | | | | | | |
| C | 34, 53 | <20 | 27 | <20 | <20 | 49 | 32 | 35 | 32 | <20 |
| N | | <20 | <20 | <20 | 81 | 8 | <20 | <20 | <20 | <20 |
| O | 10, 9 | <50 | <50 | <50 | <50 | | <50 | <50 | <50 | <50 |
| H | | <3 | <3 | <3 | <3 | | <3 | <3 | <3 | <3 |

Al, B, Be, Co, Cr, Cu, Fe, Hf, Ni, Si, Ta, Ti, W and Zr levels below 50 wppm.

in the as-received Mo–41Re alloy was performed at ORNL by electron microprobe analysis. Analysis of the carbon and oxygen levels in the as-received Mo–41Re was performed by H.C. Starck from two separate samples from the ingot [17]. Limitations on available material for chemical analysis of the annealed and aged materials prevented a more accurate determination of the interstitial levels in the two alloys. While the carbon to oxygen ratios in both alloys in the as-received condition were at or greater than 3, the mechanical properties of the alloys in this investigation are driven more by microstructural changes occurring as a result of thermal aging.

Miniature sheet tensile specimens of SS-3 geometry ($0.76 \times 1.52 \times 7.62$ mm gauge and 25.4 mm overall length) were fabricated from the as-received material using Mo-wire electrical discharge machining (EDM) with water as the cooling fluid to minimize impurity pickup. Specimens were cut so that the gage length of the tensile samples was parallel to the rolling direction of the sheet material. Following cutting, samples were polished to a 32 or better finish. In addition to the SS-3 samples additional pieces of material for metallurgical analysis were cut from the as-received material. After sample fabrication and prior to annealing, all samples were electrochemically polished and cleaned for 1 min in a solution of nitric acid, phosphoric acid, hydrofluoric acid and acetic acid [17].

### 2.2. Heat treatments

The 24 SS-3 samples and additional metallurgical samples were annealed for 1 h at 1773 K in high vacuum $1.3 \times 10^{-4}$ Pa ($1 \times 10^{-6}$ torr) prior to any long term aging. Specimens were placed inside a Nb–1Zr box in the furnace to reduce the potential for impurity pickup. Samples were furnace cooled under vacuum, by cutting current to the furnace elements; resulting in an approximate 120 K/min cooling rate from 1773 to 1273 K, 42 K/min from 1273 to 1073 K and less than 25 K/min below 1073 K.

The thermal aging treatments were conducted in parallel with radiation experiments conducted at ORNL, the results of which will be presented separately [18]. Therefore, the SS-3 samples were loaded into pure Nb holders held in place with Mo springs similar to their irradiated counterparts. The Nb holders containing the tensile specimens along with Ta foil wrapped metallurgical samples were loaded into alumina tubes with alumina end caps that were in turn placed in an alloy 600 tube and sealed by alloy 600 end caps. The superalloy capsules were welded shut under the same inert gas used in irradiation study; helium for 1098 and 1248 K aging and neon for the 1373 K aging. Prior to welding, repeated pumping and purging cycles were performed to ensure a purified atmosphere in the encapsulated cans. During each pump cycle a vacuum of approximately $1.3 \times 10^{-4}$ Pa ($1 \times 10^{-6}$ torr) was obtained. Leak checking of the sealed capsules was performed prior to aging for 1100 h in open air box furnaces at 1098, 1248 and 1398 K. The aging temperatures selected were 25 K higher than the designed irradiation temperatures used in the companion tests, based on the margin of uncertainty in the design irradiation temperatures. Temperatures in the box furnace were monitored by placing thermocouples located near the sealed capsules. The duration of all aging treatments was 1100 h.

Visual inspection of the samples aged at 1098 and 1248 K showed no signs of discoloration (oxidation/nitridation). However, upon inspection of the 1398 K aged samples, discoloration was observed on the Ta foil and Nb holders. The aged Mo–Re samples removed from the Nb holders and Ta foil did not show any visible discoloration. Investigation of the alloy 600 can aged at 1398 K showed discoloration and corrosion product on the inside of the can at one of the welded end caps. Based on further examination, the pinhole leak appears to have been formed during cooling of the can upon removal from the furnace due to thermal contractions.

Chemical analysis of the impurity levels of the annealed and aged Mo alloys was performed at Wah Chang through inert gas fusion techniques for oxygen and nitrogen, and by combustion analysis for carbon levels. The impurity elements in the alloys following 1 h anneal and 1100 h aging are presented in Table 1. Analysis of substitutional impurities (Al, B, Be, Co, Cr, Cu, Fe, Hf, Ni, Si, Ta, Ti, W and Zr) in the annealed and aged alloys was also performed and found to be below the 50 wppm detectable level. Chemical analysis showed no significant changes in the impurity pickup following annealing and 1100 h aging over the as-received values. Only a 61 wppm increase in nitrogen was measured in Mo–41Re following 1100 h aging at 1398 K.

### 2.3. Microscopy and metallographic analysis

Pieces from the annealed and aged metallographic samples were polished and examined under

back-scatter electron imaging in a Philips XL30-FEG scanning electron microscope (SEM). The metallographic samples were then etched with a solution of 60 mL $H_2O$ + 30 mL $HNO_3$ + 10 mL HF and examined by optical microscopy (OM). Samples for transmission electron microscopy (TEM) were cut by EDM and polished to less than 0.25 mm thickness and jet-polished with an electrolyte of 10 vol.% $H_2SO_4$ + 4% HF + 14% butoxy ethanol in methanol at 248 K. Samples were examined in both a Philips Tecnai T20 and CM200 FEG microscopes equipped with energy dispersive X-ray spectrometers (EDS).

EDS spectra and high-resolution spectrum profiles were taken and analyzed using the Emispec ESVision software program. Intensity spectra were corrected for background and compositions were calculated using the standardless Cliff–Lorimer ratio technique. To determine the amount of Re segregation at the grain boundaries in the as-annealed and aged Mo–41Re material, drift corrected profiles across the grain boundaries were measured using the HR-STEM mode on the CM200FEG instrument with spectra taken at intervals of 3–10 nm. Grain boundaries in the investigated samples were aligned edge-on relative to the electron beam while being tilted toward the face of the EDS detector to increase signal strength and decrease statistical error. Typical electron beam probe diameters were between 1.4 and 1.6 nm FWHM.

A total of seven hardness measurements were made on the annealed and aged tensile specimens by Buehler Micromet 3 hardness indenter equipped with a Vickers indenter tip using a 1 kg load, with a dwell time of 15 s. Typically, one specimen was analyzed for each alloy/aging combination. All indents were made on the grip regions of the SS-3 tensile specimens spaced at least 500 μm apart and well away from the gage length so that later tensile tests were not influenced. The electrochemical polishing and cleaning of the samples were sufficient to remove the deformation layer on the sample surfaces from fabrication and machining.

### 2.4. Electrical resistivity

Electrical resistivity was measured at room temperature using a four-point probe technique on the standard SS-3 tensile specimens of each alloy in the as-annealed and aged conditions, in accordance with ASTM B 193–87 [19]. A Keithley Model 238 source-measure unit is used to supply the 0.1 A current to the outer contacts near the tab regions of the SS-3 specimen, and a Keithley Model 183 sensitive digital potentiometer is used to measure the voltage drop between the inner contacts spaced 6.46 mm apart in the gage section of the tensile samples. The accuracy of both the potential measurement and current sourcing is rated as <0.1%. The samples behave in an Ohmic fashion for varied applied currents. Possible sample orientation effects have been eliminated in that data is reproducible for different sample orientations (flipped or flipped and rotated). A minimum of five measurements were taken on each specimen. The measured voltage drop was readily converted to resistivity with a temperature of 294.6 K (room temperature) chosen as the reference temperature for the calculation. The resistivity is calculated from the measured voltage drop using

$$\rho_{294.6}(\text{n}\Omega\text{-m}) = \frac{(V \times A)}{(I \times L)(1 + \alpha(T_{\text{m}} - 294.6))}, \qquad (1)$$

where $\rho_{294.6}$, resistivity in nΩ-m at the reference temperature of 294.6 K; $V$, measured voltage at the measurement temperature (nV); $A$, cross-sectional area of sample in ($m^2$); $I$, applied current (0.1 A); $L$, distance between inner electrodes = 0.00646 m for SS-3 sample holder; $\alpha$, temperature coefficient of electrical resistivity; $T_{\text{m}}$, temperature of measurement (K).

For each specimen, the cross-sectional area was measured using a calibrated micrometer with 1 μm or better resolution. The width of the gage section was measured at the center of the gage section and the specimen thickness was measured at two locations along the gage length. The temperature was measured before and after electrical measurements on each set of specimens. The temperature coefficient of electrical resistivity, $\alpha$, was selected as 0.0044 $K^{-1}$ which is the value for pure Mo ($\alpha$ for pure Re = 0.0045 $K^{-1}$) [20]. Before and after measurements of the Mo–Re samples, the system calibration was tested against a pure Cu specimen (99.999%).

The measured values of electrical resistivity were made for the purpose of comparing the changes occurring between the as-annealed and aged conditions rather than an absolute value of resistivity. Therefore, dissimilar metal voltages and contact resistances are not considered. In addition, the use of electrical contacts or solders was avoided so as not to influence tensile tests and for experimental

simplicity in performing measurements on the irradiated companion samples of these specimens.

### 2.5. Tensile properties

Tensile testing has been performed on the as-annealed and aged SS-3 specimens and following ASTM standard E8-04 [21]. Yield stress (YS), ultimate tensile stress (UTS), and uniform and total elongation were determined for each test. Tests at room temperature and above were performed using a United Technology System SFM-10 test frame, equipped with a Thermal Technology vacuum furnace. Tensile tests were performed at a crosshead speed of 0.0076 mm/s (0.018 in./min), corresponding to a nominal strain rate of $\sim$0.001 $s^{-1}$. Testing of the aged samples was performed at the same targeted temperatures as their companion irradiated samples (1073, 1223, or 1373 K). Temperatures were measured using a type-C thermocouple positioned within 2 mm of the gauge section. Room temperature tests were conducted in air, while elevated temperature testing was in vacuum. Vacuum pressure during elevated temperature testing was maintained at $2 \times 10^{-4}$ Pa ($2 \times 10^{-6}$ torr) or lower.

## 3. Results and discussion

The microstructural and mechanical property changes occurring in the Mo-base alloys as a result of aging from the annealed condition are presented. The results from optical (OM) and electron microscopy (EM) analysis are discussed for the individual alloys. In addition, the changes in electrical resistivity, hardness and tensile properties due to thermal aging are presented.

### 3.1. Mo–41Re alloy

#### 3.1.1. Microstructural examination

Samples of the Mo–41Re alloy were prepared for OM and EM characterization from the 1773 K as-annealed material and the three 1100 h aging conditions. Representative microstructures of the as-annealed and 1248 K aged materials are shown in Fig. 1. Examination of the as-annealed and 1100 h aged samples showed single-phase microstructures with equiaxed grains and uniform size distribution. A mean grain diameter of 24 μm for both the as-annealed and aged samples was measured by the line-intercept technique. Investigation of the

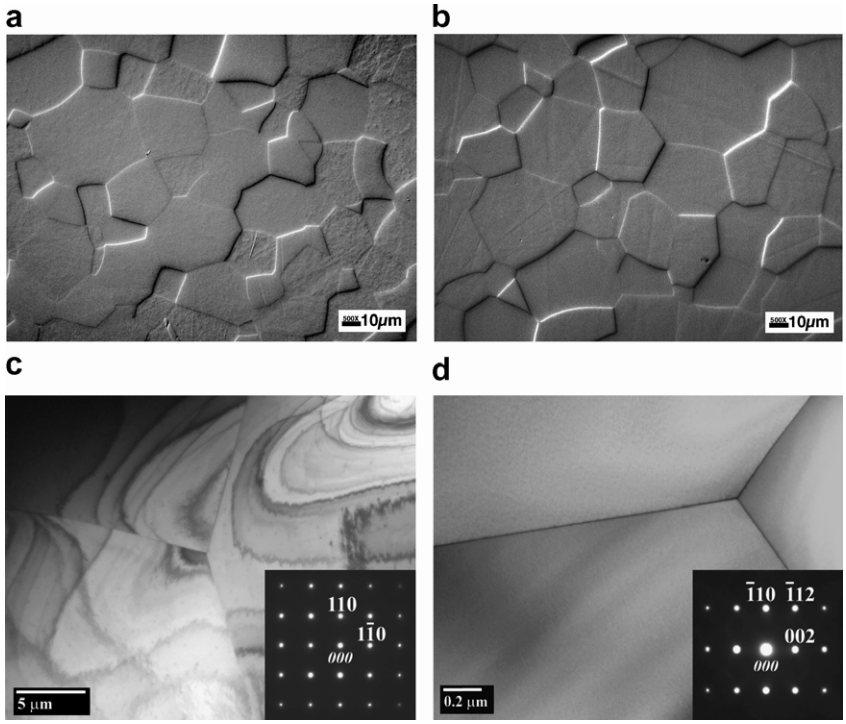


Fig. 1. Representative microstructures of Mo–41Re alloy. Optical micrographs of the (a) as-annealed and (b) 1248 K aged materials. TEM micrographs of the (c) as-annealed and (d) 1248 K aged materials, with inserts showing the [0 0 1] and [1 1 0] zone axes patterns, respectively.

as-annealed and 1100 h aged materials showed no evidence of precipitation in the materials.

Examples of TEM micrographs showing grain boundary tri-junctions in the as-annealed and 1248 K aged samples are shown in Fig. 1(c) and (d), respectively. Selected area diffraction (SAD) patterns of the [001], [110] and [111] zone axes were examined from each of the annealed and aged samples. Representative SAD patterns of the [001] and [110] zone axes are shown as inserts in the TEM micrographs of Fig. 1(c) and (d), respectively. The SAD patterns include only diffracting planes from the bcc solid solution αMo phase. Furthermore, no streaking or super-lattice reflections were observed in the diffraction patterns to suggest any decomposition or ordering of the solid solution phase. The single-phase solid solution structures observed in the as-annealed and aged samples correlates with work by Nemoto et al. [22] on Mo–Re alloys, in which no evidence of precipitation of secondary phases were observed in Mo–41Re aged for 720 h at temperatures up to 1073 K by either TEM or X-ray diffraction techniques.

High-resolution EDS profiles across the grain boundaries in the as-annealed and aged samples showed a small amount of Re segregation when compared to the bulk composition values. The average grain boundary Re content in the as-annealed material was measured at $43.1 \pm 0.4$ wt% and increased slightly to an average of $44.4 \pm 0.4$ wt% for the aged samples. The uncertainty represents the standard deviation of the mean. Average background matrix concentrations away from the grain boundary were measured near $40.7 \pm 0.4$ wt% Re for the as-annealed Mo–41Re, correlating with chemical analysis. The average background matrix for the aged materials was measured at a slightly lower concentration of $40.5 \pm 0.3$ wt%, but was still statistically the same as the annealed material. Profiles of the grain boundary scans for the several conditions are presented in Fig. 2. While there was an increase in the Re concentration at the grain bound-

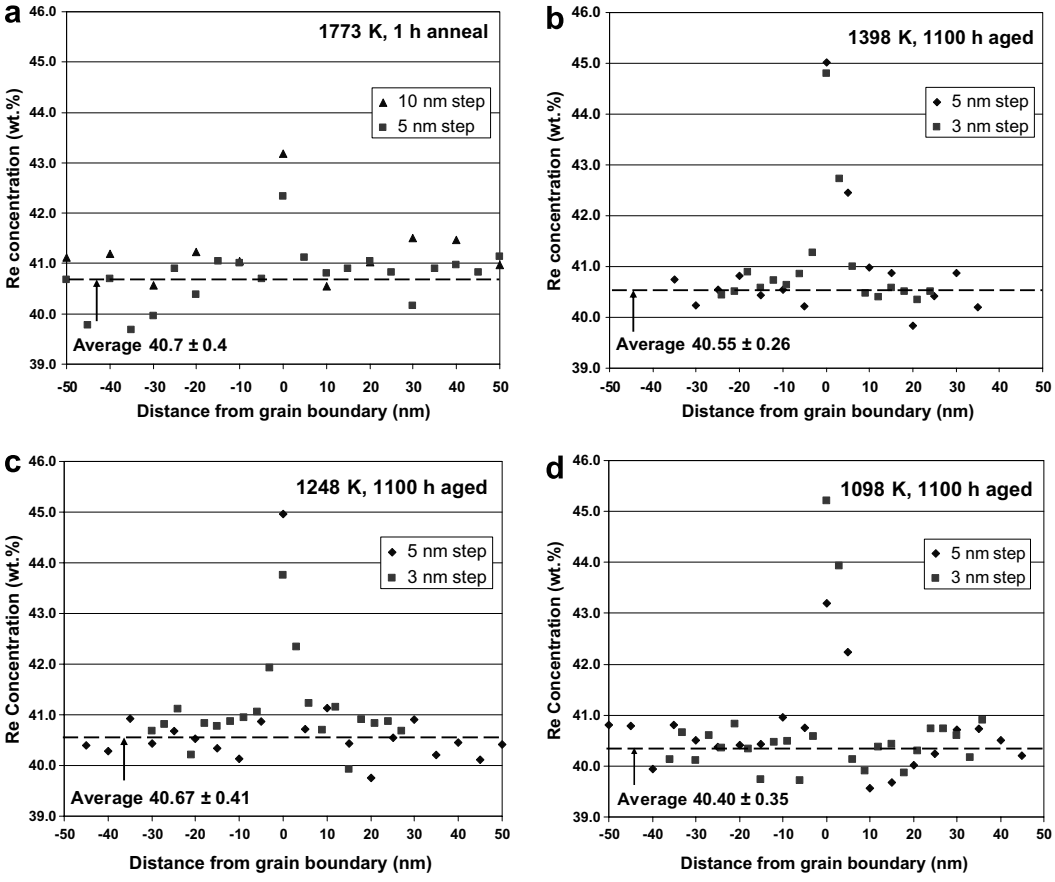


Fig. 2. Rhenium concentration profiles across grain boundaries in Mo–41Re in the (a) as-annealed condition, (b) 1398 K aged, (c) 1248 K aged and (d) 1098 K aged materials. Average bulk concentrations of the solid solution are marked in each plot.

aries of the aged material, no correlation or trend was observed relative to aging temperature itself. In general, good agreement was observed between the different step rates across the selected profiles for a given material despite a slight overlap between sampled points along the profile for the 3 nm step size.

### 3.1.2. Mechanical properties

The room temperature resistivity of the annealed and aged Mo–41Re (Table 2) matches reasonably well with the reported literature value of 202 nΩ-m at 373 K [23], despite the differences in referenced temperatures. For the Mo–41Re alloy, a decrease in electrical resistivity from the as-annealed value was measured with decreasing aging temperature; with the averaged value of resistivity of the 1398 K aged material approaching that of the as-annealed condition. These changes correlated with increases in hardness (Table 3) with decreasing aging temperature and may be related to the distributions of interstitials in the alloy.

Significant differences were not observed in the tensile properties of Mo–41Re between the as-annealed and the 1098 and 1248 K aged materials (Table 3). However, an increase in the yield and ultimate tensile strengths of the 1398 K aged material over the as-annealed was measured. The electronic data file for the 1398 K aged specimen (M139) was corrupted and not available for direct graphical comparison with the annealed specimen. The raw stress–strain curves for the as-annealed and 1098 K aged samples tested at 1073 K are presented in Fig. 3. Both conditions exhibit a slight yield drop followed by a limited Luders strain region. In addition, both samples displayed dynamic strain aging during plastic deformation at plastic strains greater than the Luders strain. This was observed at all test conditions for both the as-annealed and aged materials. A slight reduction in the uniform elongation was observed for the 1398 K sample, though these properties represent only one test conducted at this time and may have been the result of the slight increase in $N$ level in the alloy measured by chemical analysis (Table 1). However, the level of $N$ is still relatively low. Nevertheless, adequate uniform and total elongation values are observed. In addition, the measured changes in resistivity and hardness between the 1398 K aged and as-annealed samples were insignificant. All Mo–41Re tensile tests showed transgranular ductile failure with fractures taking place in the gage region.

The mechanical properties of the aged and annealed Mo–41Re as a function of test temperature are plotted in Fig. 4 against the data of Leonhardt et al. [24] for annealed Mo–41Re. The tensile properties of Mo–41Re of this study were found to be in excellent agreement with those of Leonhardt et al., which also reported a slight reduction in uniform elongation of the as-annealed material tested at 1475 K.

## 3.2. Mo–47.5Re alloy

### 3.2.1. Microstructural examination

Samples of the Mo–47.5Re alloy were prepared for OM and EM characterization from the 1773 K as-annealed and 1100 h aged materials. Aging of the materials resulted in precipitate development, while no statistical change occurred in the 24 μm mean diameter of the solid solution grains. Although, changes in grain size were not expected given that aging temperatures were between 0.3 and 0.5 of the melting temperature.

TEM examination of the Mo–47.5Re annealed 1 h at 1773 K revealed the presence of particles

Table 2
Room temperature electrical resistivity of Mo–41Re in the as-annealed and aged conditions

| Sample ID | As-annealed resistivity (nΩ-m) | Resistivity after 1100 h aging at (nΩ-m): | | | Change due to aging (nΩ-m) |
|---|---|---|---|---|---|
| | | 1098 K | 1248 K | 1398 K | |
| M131 | 182.7 | 179.2 | | | −3.5 |
| M132 | 186.6 | 183.6 | | | −3.0 |
| M133 | 181.5 | 178.2 | | | −3.3 |
| M134 | 182.4 | | 179.7 | | −2.7 |
| M135 | 185.9 | | 182.9 | | −3.1 |
| M136 | 183.3 | | 180.8 | | −2.4 |
| M137 | 186.0 | | | 185.5 | −0.5 |
| M138 | 185.0 | | | 184.4 | −0.6 |
| M139 | 182.8 | | | 182.3 | −0.5 |

Table 3
Hardness and tensile properties of annealed and 1100 h aged Mo–41Re

| Test temperature (K) | Condition | Hardness ($kg/mm^2$) | Sample ID | YS (MPa) | UTS (MPa) | Uniform elongation (%) | Total elongation (%) | Reduction in area (%) |
|---|---|---|---|---|---|---|---|---|
| RT | Annealed | 321 ± 5 | M125 | 769 | 900 | 17.2 | >25 | – |
| | Aged 1098 K | 340 ± 6 | M131 | | | | | |
| | Aged 1248 K | 323 ± 4 | M135 | | | | | |
| | Aged 1398 K | 320 ± 4 | M139 | | | | | |
| 1073 | Annealed | | M130 | 303 | 503 | 17.9 | 30 | 93.5 |
| | Aged 1098 K | | M132 | 294 | 500 | 19.2 | 30.6 | 93.3 |
| 1223 | Annealed | | M127 | 275 | 393 | 16.8 | 39 | 98.8 |
| | Aged 1248 K | | M136 | 265 | 398 | 16.8 | 35.1 | 96.1 |
| 1373 | Annealed | | M126 | 228 | 275 | 11.7 | 50.5 | 80.6 |
| | Aged 1398 K | | M139 | 241 | 300 | 9.4 | 62.3 | 91.3 |

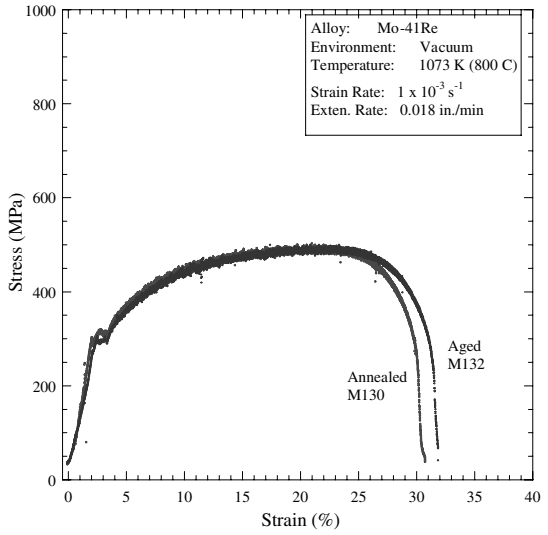


Fig. 3. Comparison of the stress–strain curves for 1098 K aged and as-annealed Mo–41Re samples tested at 1073 K.

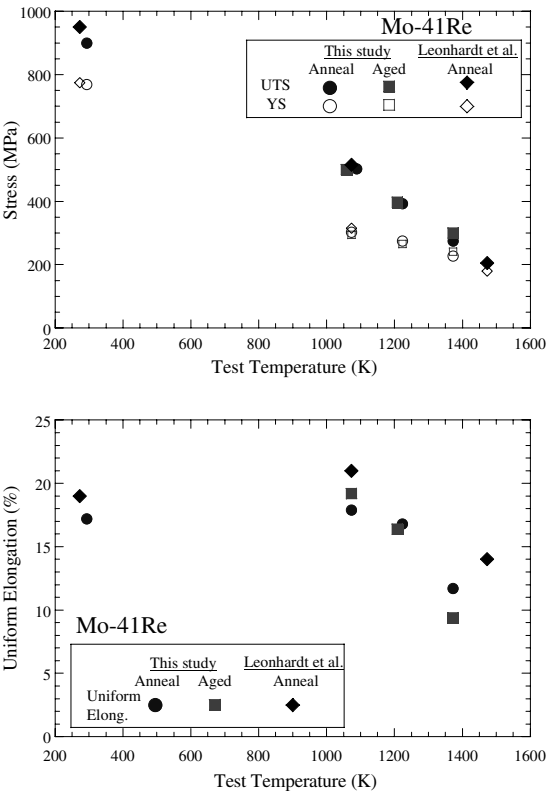


Fig. 4. Comparison of mechanical properties of annealed and aged Mo–41Re samples of this study with literature results [24].

along the grain boundaries, grain boundary triple junctions and in the grain interiors (Fig. 5). These particles were identified as σ through electron

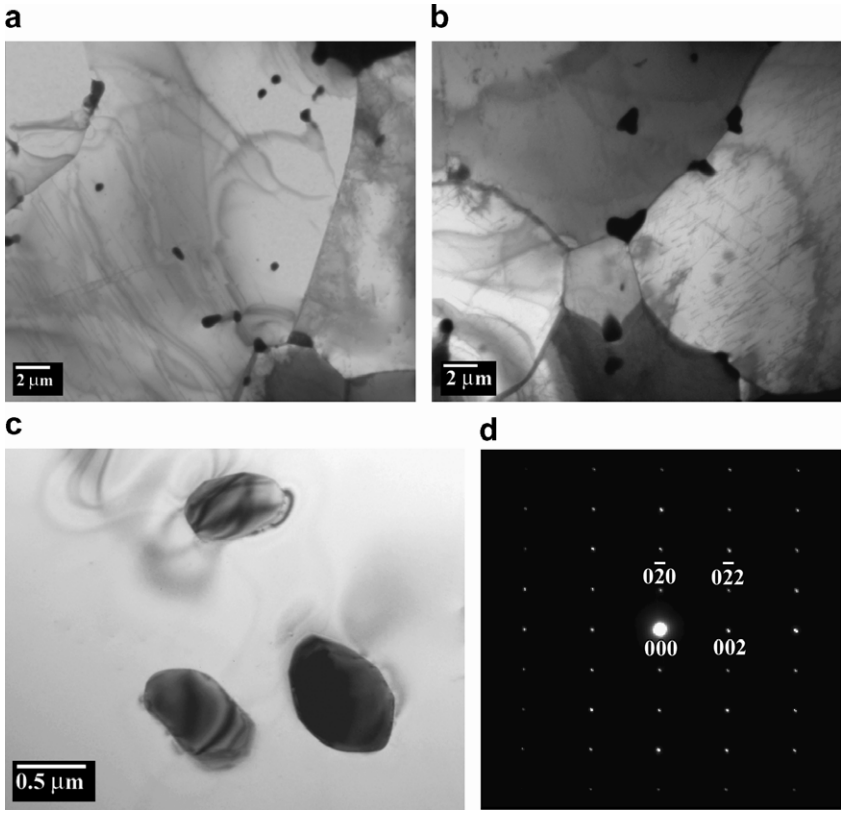


Fig. 5. TEM micrographs of Mo–47.5Re annealed 1 h at 1773 K. (a, b) Low magnification images showing σ phase particles along grain boundaries and inhomogeneously distributed throughout grain interiors. (c) Three σ phase particles observed in the interior of a matrix grain that were once part of a larger particle. (d) The [100] SAD pattern identifying the σ phase in the annealed material.

diffraction, Fig. 5(d) and ranged in size from 0.5 to 2.0 μm with a rounded or globular morphology. Compositions of the solid solution and σ phase of the as-annealed material is presented along with the phases present following 1100 h aging in Table 4. In the as-annealed material, no significant difference in composition was observed between the σ phase particles located on the grain boundaries to those of the grain interiors, though the measured composition of σ had a larger statistical variation than that of the αMo solid solution phase. The variations in composition listed in Table 4 are based on the range of data over the average and not on the actual error in the quantified spectra. For certain phases appearing in the Mo–47.5Re samples, the actual range of data are provided. Data sets were taken from both the T20 and CM200 microscopes for each heat treatment condition, with the averaged values presented in Table 4. The data is further graphically illustrated

Table 4
Quantitative analysis of the phases present in the as-annealed and aged Mo–47.5Re alloys

| Condition | Phase | Composition (wt% Re) |
|---|---|---|
| Annealed 1 h at 1773 K | Solid solution | 42.5 ± 0.7[a] |
| | σ phase | 67.9 ± 2.9 |
| Aged 1100 h at 1398 K | Solid solution | 41.1 ± 0.8 |
| | σ phase | 66.6 ± 1.4 |
| Aged 1100 h at 1248 K | Solid solution | 42.0 ± 0.6 |
| | χ phase | 79.3 ± 1.0 |
| | Re-lean[b] | 5–29 (14 ave.) |
| Aged 1100 h at 1098 K | Solid solution | 42.6 ± 3.2 |
| | σ phase | 73.6 ± 0.2 |
| | χ phase | 76.2 ± 1.6 |
| | Re-lean[b] | 15–20 (18 ave.) |

[a] Variation in composition is based on the range of data from the average and not the actual error in the quantified EDS spectra.
[b] Large variation observed in composition, range of data is provided with average shown in parentheses.

against the most recent published Mo–Re binary diagrams [25,26] in Fig. 6. The Mo–Re diagram of [26] shows the Mo–47.5Re alloy lying outside the αMo + σ phase field, contrary to this and other existing work. The presence of the σ phase in the 1773 K annealed material and the resulting tie-line compositions suggest that the boundary of the Re solubility in the αMo phase is of a leaner Re concentration than shown in either diagrams.

A group of three σ particles was observed in a region of the 1773 K annealed material which was once part of a larger σ particle (see Fig. 5(c)). This conclusion was based on all three particles exhibiting the exact same crystallographic orientation in the solid solution matrix relative to each other when examined through diffraction techniques. The matrix concentration between the particles was approximately 2.3 wt% richer in Re than the average composition away from the particles, suggesting that the phase boundaries were still shifting during the 1 h anneal and that the σ phase particles in the microstructure did not form on furnace cooling from 1773 K.

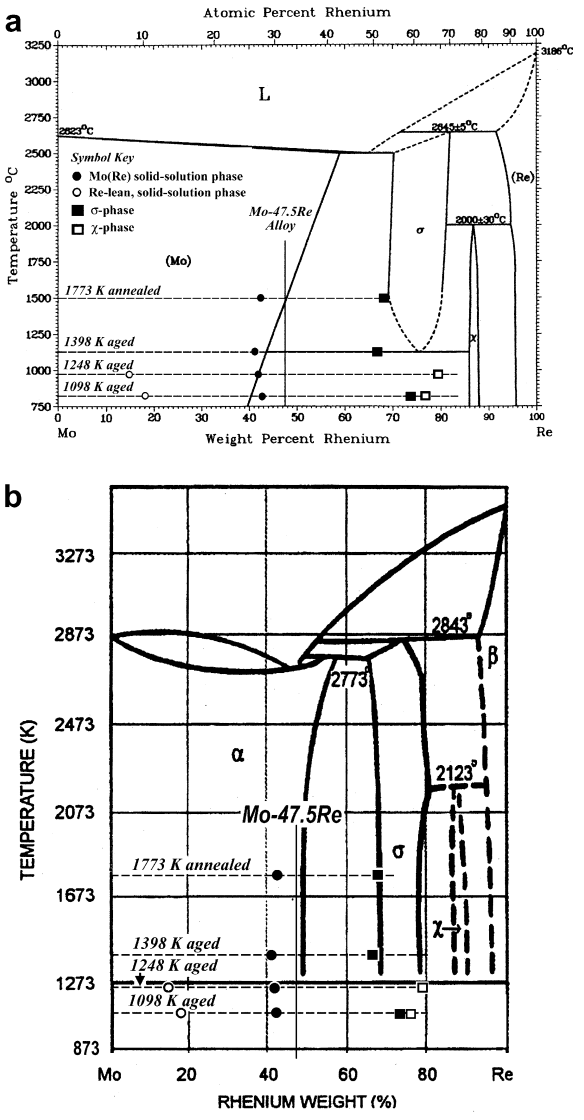


Fig. 6. Composition data for the Mo–47.5Re alloys measured by TEM examination, shown as measured points superimposed on the Mo–Re binary phase diagrams from (a) Ref. [25] and (b) Ref. [26]. The temperature axis in (b) was extended to incorporate the 1098 K data.

The exact temperature at which the Mo–47.5Re alloy crosses into the single-phase αMo solid solution region is not precisely known. A limit of Re solubility in Mo–47.5Re of 1748 K, below which the alloy falls into the two-phase αMo + σ phase field, is shown by the Mo–Re binary in Ref. [25]. However, work by Shields [27] on Mo–47.5Re has also shown that σ phase particles are present in the microstructure following a 1 h anneal at 1773 K through OM examination, with X-ray diffraction indicating a single αMo phase was achievable after 1 h annealing at 1873 K. Though unsubstantiated, traces of σ phase remaining in the structure following 2.7 h annealing at 1873 K were reported [26]. For comparison, a single-phase Mo–45Re alloy was produced following a 5 h anneal in vacuum at 1973 K [28]. Nonetheless, the 1773 K anneal of Mo–47.5Re in this study has yielded a two-phase structure. Therefore, some amount of σ can be expected in the aged samples due to the incomplete resolution.

Electron microscopy of the 1398 K aged material revealed further development and precipitation of the σ phase along the solid solution grain boundaries. Low magnification images of the structures observed in the SEM and a representative higher magnification image from TEM is shown in Figs. 7 and 8, respectively. Examination of the particles by electron diffraction, insert shown in Fig. 8, confirmed the σ phase. The formation of σ was predominantly along the grain boundaries with only a sparse inhomogeneous distribution of particles in the solid solution grains. No other precipitate phases were identified in the sample, suggesting that the slow cooling rate of the encapsulated samples was sufficient enough to prevent χ phase precipitation.

The 1398 K aged sample showed more angular or faceted surface morphology of the σ phase particles and grains than those appearing in the as-annealed

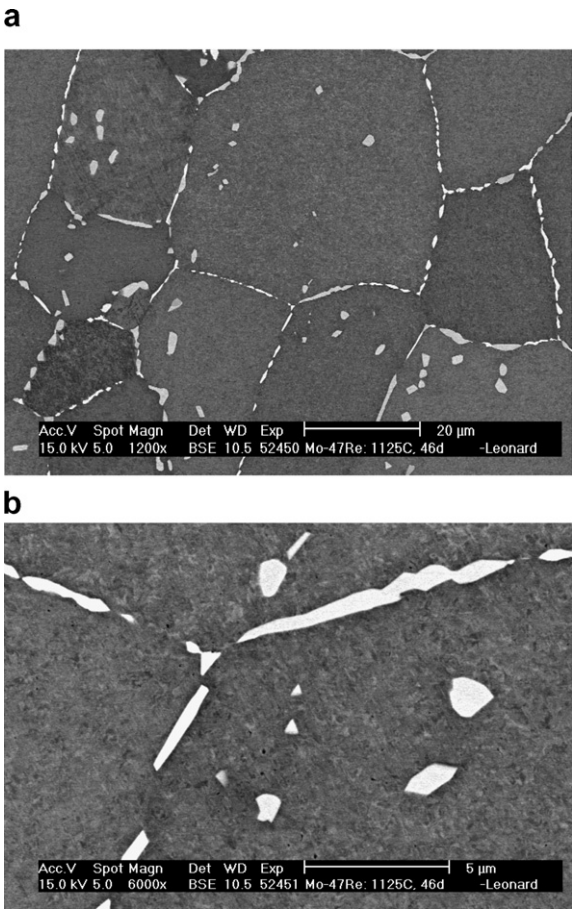


Fig. 7. (a) Low and (b) higher magnification back-scatter electron SEM images showing σ phase development in Mo–47.5Re aged 1100 h at 1398 K.

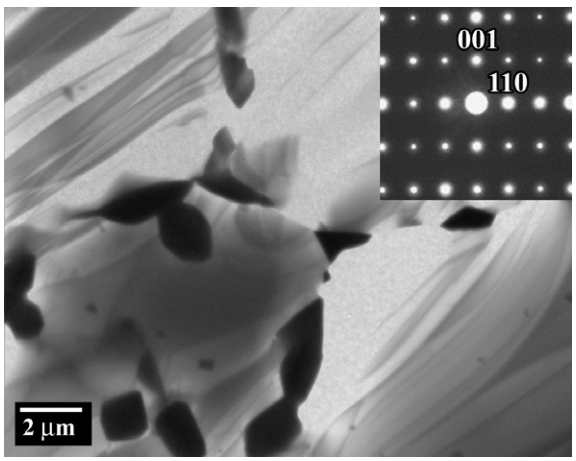


Fig. 8. TEM image of σ phase precipitation in Mo–47.5Re aged 1100 h at 1398 K, with insert showing the [1 1 0] SAD pattern of the σ phase.

material. This correlates with nucleation and growth of the σ phase at the lower temperature. The angular particle morphology of the σ phase was first reported on by Ogawa and Maddin [29] for a Mo–50(wt%)Re alloy. In which a $\sigma[1\,0\,0]\|\|\mathrm{Mo}[1\,0\,0]$ orientation relationship was observed between the particles and matrix, with the habit plane of the σ phase and the edges of the particles determined to be along the $\{1\,1\,0\}$ and $\langle 1\,1\,1\rangle$ of the matrix, respectively. The strong orientation relationship between σ particles and the αMo matrix is further illustrated through electron diffraction in Fig. 9. In this study, particles were observed to show a near $\sigma[1\,1\,1]\|\alpha\mathrm{Mo}[1\,1\,1]$ orientation to the matrix, with the $\sigma[1\,1\,1]$ zone being tilted approximately 3° from the αMo zone axis. However, the $\sigma(1\,\bar{1}\,0)\|\alpha\mathrm{Mo}(1\,\bar{1}\,0)$ habit relationship between the particle and the solid solution matrix was observed, with the $\{1\,1\,0\}\sigma$ reflections of the habit plane appearing at $1/3\{1\,1\,0\}\alpha\mathrm{Mo}$ positions. The surfaces of the σ-particle shown in Fig. 9(b) was determined to be along $\langle 1\,1\,0\rangle$ and $\langle 1\,0\,1\rangle$ directions, with the earlier matching with $\alpha\mathrm{Mo}\langle 1\,1\,0\rangle$ of the matrix.

Similar to 1398 K aged material, the 1248 K aged Mo–47.5Re material shows near complete grain boundary coverage by precipitates throughout the microstructure (Fig. 10). However, several characteristic features distinguish the 1248 K aged material from that of the 1398 K aged condition. These include an apparent decrease in the volume fraction of precipitation occurring along the grain boundaries, the lack of precipitation in the grain interiors and the additional appearance of a dark-contrasting phase at the grain boundaries appearing in the back-scatter electron (BSE) SEM images.

The precipitate structure along the grain boundaries of the solid solution phase were examined through TEM (Fig. 11) and identified through electron diffraction analysis as the cubic ($I\bar{4}3m$) structured χ phase. The χ phase was found to develop only along the grain boundaries of the solid solution matrix. No precipitation in the solid solution matrix grains was observed either by TEM or SEM analysis. In addition, σ phase particles were not identified during TEM analysis of the three prepared foils, this despite the as-annealed material containing the σ phase. The appearance of the two-phase $\alpha\mathrm{Mo} + \chi$ phase field correlates with one of the published binary phase diagrams [25], but contradicts that presented by Carlen and Bryskin [26] which shows the extension of the σ phase field to temperatures below 1398 K. Work by Mannheim and Garin [30]

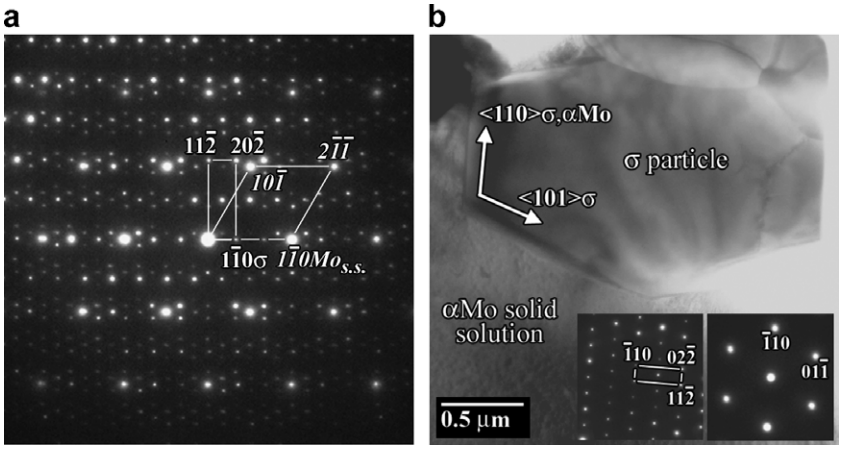


Fig. 9. TEM micrographs illustrating σ particle morphology in Mo–47.5Re aged 1100 h at 1398 K. (a) SAD pattern showing the $\alpha Mo[1\,1\,1]\|\sigma[1\,1\,1]$, $\alpha Mo(1\,\bar{1}\,0)\|\sigma(1\,\bar{1}\,0)$ orientation relationship between a particle and the αMo solid solution ($Mo_{s.s.}$) taken at the interface, with the primary repeating patterns identified. Additional reflections present are due to double diffraction. (b) Bright-field image of σ particle showing $\langle 1\,1\,0\rangle$ and $\langle 1\,0\,1\rangle$ surface features with representative tilt corrected SAD patterns of the $\sigma[1\,1\,1]$ and $\alpha Mo[1\,1\,1]$ zone axis. The $\sigma[1\,1\,1]$ zone axis of the particle is approximately 3° off the $\alpha Mo[1\,1\,1]$ zone.

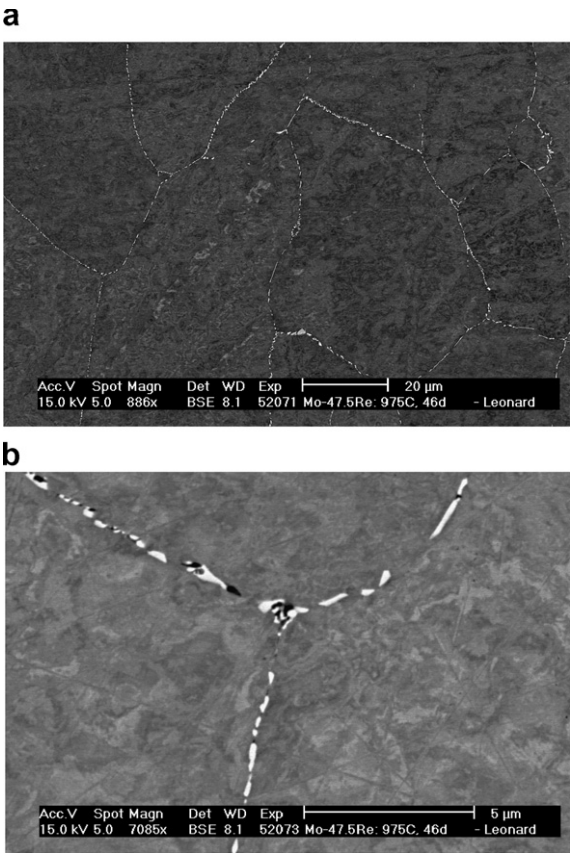


Fig. 10. (a) Low and (b) higher magnification back-scatter electron SEM images of χ phase precipitation in Mo–47.5Re aged 1100 h at 1248 K.

on Mo–Re alloys further provides supporting evidence for an $\alpha Mo + \chi$ phase field. In Mo-(40–50)Re samples cooled at a rate of 4 K/min from 2023 K increasing amounts of the σ and χ phases were measured through X-ray diffraction with increasing levels of Re in the alloy. The presence of the σ phase in their work was characterized as a metastable structure remaining from the high temperature phase field due to the slow kinetics of the system. However, the appearance of the χ phase suggests that a phase boundary was crossed on cooling.

The dark-contrasting features appearing in BSE-imaging (Fig. 10(b)) were identified as additional grains of the bcc solid solution that have developed adjacent to the χ phase particles (Fig. 11). However, these additional grains showed a composition that was lean in Re relative to the bulk solid solution. Hence, the dark appearing features in the BSE-images. The average concentrations of the Re-lean grains were near 15 wt% Re, but showed a large compositional range over the numerous particles measured (Table 4). The spread in composition measured for the Re-lean grains was due to the relatively small size of the particles resulting in unwanted beam interactions with its Re-rich surroundings and to the non-equilibrium nature of the structure. Differences in the concentration of interstitials between the Re-lean grains and the αMo grains were not detectable. The Re-lean grains may be the result of depletion of Re to the forma-

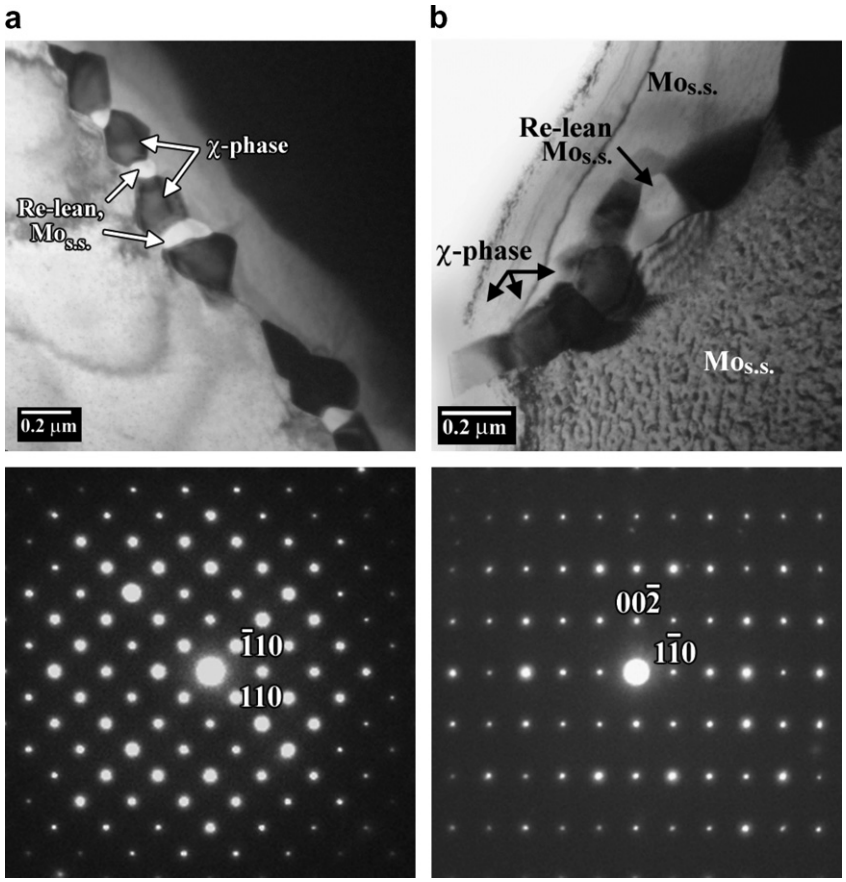


Fig. 11. (a, b) TEM micrographs of χ phase formation along the solid solution ($Mo_{s.s.}$) grain boundaries in Mo–47.5Re aged 1100 h at 1248 K. Micrographs show the additional formation of grains of Re-lean solid solution between the χ grains. The (a) [0 0 1] and (b) [1 1 0] SAD patterns of the χ phase.

tion of the stable χ phase. However, the sharp demarcation between the Re-lean grains and the surrounding solid solution grains is puzzling, suggesting a possible role of interstitials or a more complex dependence for interdiffusion.

In addition to the tabulated composition data (Table 4) the measured compositions of the solid solution, χ and Re-lean phases of the 1248 K aged material are plotted on the binary phase diagrams in Fig. 6. The distinct change in volume fraction of the precipitate phase covering the grain boundaries between the 1248 and 1398 K aged materials was the result of the shifting of the tie-line to higher Re concentrations associated with the χ phase precipitation at 1248 K. However, the solid solution matrix phase composition at 1248 K was determined to be richer in Re than expected based on the results of the data from the 1398 K aged and 1773 K annealed materials. The composition of the solid solution phase approaching that of the αMo solvus line at 1248 K of Ref. [25] (Fig. 6(a)), may be the result of the alloy not having reached equilibrium even after 1100 h. It is expected that as the χ phase further develops and grains of the Re-lean phase disappear, the tie-line compositions for the αMo and χ phases may further separate to lower and higher Re concentrations, respectively. To date no study has concentrated on the growth kinetics of either the σ or χ phases.

Microstructural examination of the 1098 K aged samples showed the remains of the as-annealed structure along with the developing low temperature phase equilibria. BSE-imaging revealed irregular shaped particles averaging 1 μm in size distributed inhomogeneously throughout the solid solution matrix (Fig. 12). Closer examination revealed changes occurring at the interface between these particles and matrix and along the solid solution

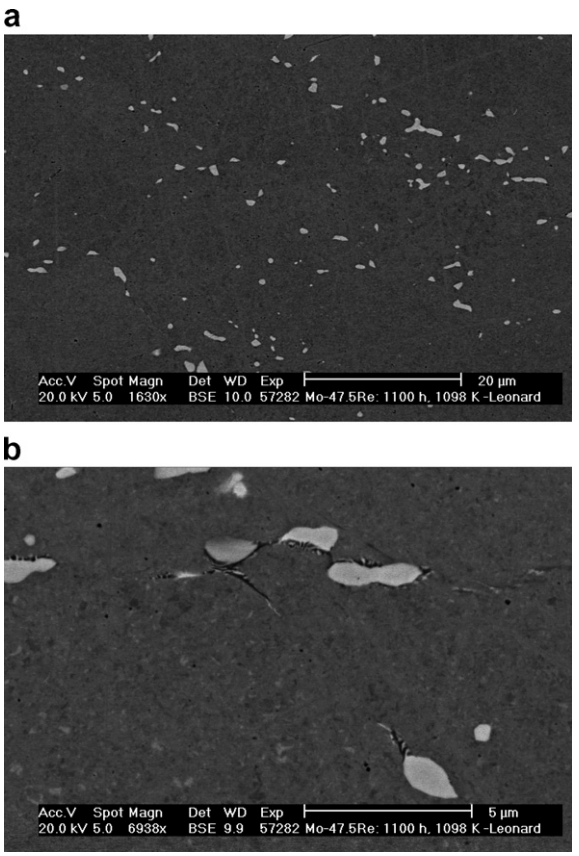


Fig. 12. (a) Low and (b) higher magnification back-scatter electron SEM images of Mo–47.5Re aged 1100 h at 1248 K. Large particles are σ, with χ phase precipitation occurring along some of the particle interfaces with the matrix.

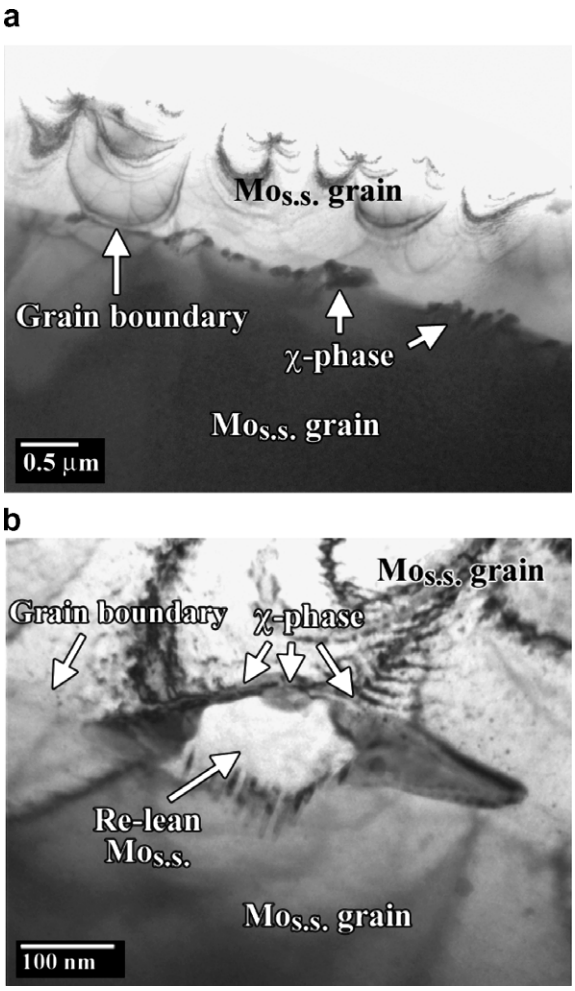


Fig. 13. (a) Low and (b) higher magnification TEM micrographs of Mo–47.5Re aged 1100 h at 1098 K showing χ phase precipitation at the solid solution ($Mo_{s.s.}$) grain boundary.

grain boundaries. TEM examination confirmed the large particles as the σ phase. The σ phase was observed at locations along grain boundaries and in the grain interiors and are the remnants of the as-annealed structure which, due to the slow kinetics at 1098 K, have not redissolved into the matrix. The slow kinetics in the system may have been a source of confusion and a possible cause for the differences in the Mo–Re binary diagrams shown in Fig. 6.

The χ phase was observed through TEM analysis along the grain boundaries of the 1098 K aged sample, Fig. 13. Typical particle size of the χ phase was less than 0.1 μm, with the χ particles being accompanied by Re-lean grains of the solid solution phase similar to the 1248 K aged material. Based on SEM examination, the χ and Re-lean grains appear to have nucleated and grown from the interfaces of the remnant σ particles as well. However, this did not occur on all of the σ particles and was not observed during TEM analysis.

The compositions of the solid solution, χ, Re-lean, and σ phases in the 1098 K aged material are presented in Table 4 and graphically on the Mo–Re-phase diagrams in Fig. 6. Despite the phases being correctly identified through their diffraction patterns prior to EDS analysis, only a 3 wt% Re difference in composition was measured between the σ and χ phases. The small size of the χ phase particles are likely to have skewed the measured composition to lower Re concentrations due to overlap of the electron beam interaction zone with the solid solution matrix. Similarly, the correct composition of the Re-lean grains may have also been skewed to higher Re concentrations than their

actual chemistry. In both cases a significant variation in composition was measured in a particle to particle analysis.

Compositional variation was also observed in the Re concentration of the solid solution phase which was found to be dependent on the examined TEM foil. The sample which contained σ particles showed Re-leaner concentrations of the solid solution phase than the TEM foil containing only the χ phase particles. Interestingly, the averaged solid solution composition is unchanged from that of the as-annealed material. Therefore, it is not unexpected that 1100 h aging at 1098 K or for that matter at any of the aging temperatures was sufficient enough for the material to reach equilibrium. Certainly, in order to verify the chemical compositions of the χ, Re-lean and σ phases in the 1098 and 1248 K aged alloy, extraction of these phases from the surrounding matrix is needed. However, several attempts at this have been unsuccessful due to the similar chemical potentials of the various phases and the αMo solid solution.

The χ phase appearing in both the 1098 and 1248 K aged samples displayed a strong orientation relationship to the parent solid solution grain. Fig. 14 illustrates this orientation relationship with the bcc solid solution phase. The cubic χ phase has a lattice parameter near $a_0 = 0.955$ nm, which is approximately 3 times that of the Mo–47.5Re solid solution ($a_0 = 0.301$ nm [31]). This results in the $\sim 1/3\{hkl\}$ diffracted spots appearing with those of the solid solution phase in the diffraction patterns. The orientation relationship can be expressed as follows for the two phases:

$$\chi[1\,1\,0] \| \alpha\mathrm{Mo}[1\,1\,0], \quad \chi(0\,0\,1) \| \alpha\mathrm{Mo}(0\,0\,1);$$
$$\chi[1\,1\,1] \| \alpha\mathrm{Mo}[1\,1\,1], \quad \chi(1\,1\,0) \| \alpha\mathrm{Mo}(1\,1\,0).$$

This cube-on-cube orientation was also reported by Erck and Rehn [28] for ion-irradiated Mo-(42–45 wt%)Re. In general, the Re-lean grains appearing with the χ phase at the grain boundaries did not share a precise relationship to either the solid solution grains on opposite sides of the boundary or to the χ phase. However, a common {100} or {110} interface with one of the larger αMo grains has been observed in this study.

### 3.2.2. Mechanical properties

The changes in the electrical resistivity and mechanical properties following 1100 h aging were found to correlate directly with precipitate development in the Mo–47.5Re alloy. The room temperature electrical resistivity values for Mo–47.5Re in the as-received, annealed and aged conditions are presented in Table 5, while hardness and tensile properties are listed in Table 6. The as-annealed resistivity for Mo–47.5Re matches well with the reported literature value of 193 nΩ-m at 293 K [23]. The formation of the χ phase in the 1098 and 1248 K samples produced an increase in the hardness of the alloy over that of the as-annealed condition, while producing a decrease in electrical resistivity specifically in the 1248 K aged material. The small amount of χ formation in the 1098 K aged Mo–47.5Re and relatively unchanged values in resistivity and hardness over the as-annealed condition, suggests that the dominant microstructural feature controlling mechanical properties was the

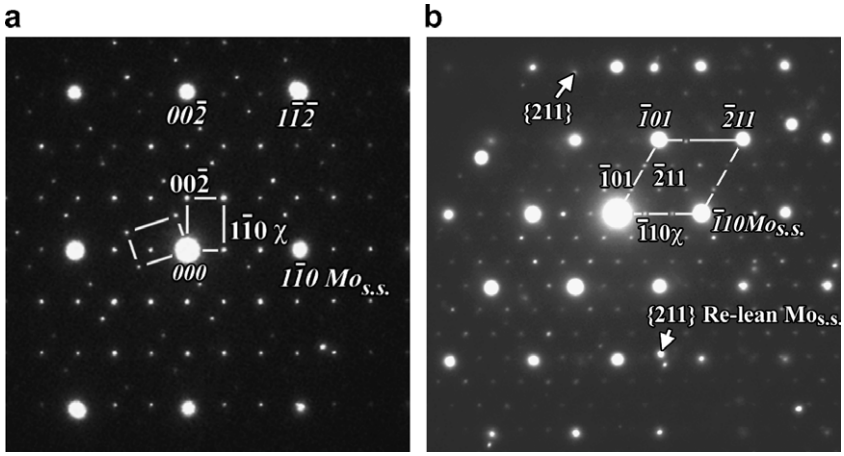


Fig. 14. SAD patterns illustrating the orientation relationship to the αMo solid solution phase ($Mo_{s.s.}$, indices shown in italic): (a) two variants of the χ[1 1 0] with the αMo[1 1 0] zone axis, and (b) the χ[1 1 1]||αMo[1 1 1] orientation relationship.

Table 5
Room temperature electrical resistivity of Mo–47.5Re in the as-received, annealed and aged conditions

| Sample ID | As-received resistivity (nΩ-m) | As-annealed resistivity (nΩ-m) | Resistivity after 1100 h aging at (nΩ-m): | | | Change due to aging (nΩ-m) |
|---|---|---|---|---|---|---|
| | | | 1098 K | 1248 K | 1398 K | |
| R731 | 196.8 | 194.4 | 194.6 | | | 0.2 |
| R732 | 199.6 | 194.6 | 195.2 | | | 0.6 |
| R733 | 198.9 | 194.6 | 195.0 | | | 0.4 |
| R734 | 197.8 | 193.4 | | 195.6 | | 2.2 |
| R735 | 197.0 | 193.1 | | 194.9 | | 1.8 |
| R736 | 203.0 | 198.3 | | 200.2 | | 1.9 |
| R737 | 198.2 | 193.3 | | | 201.3 | 8.0 |
| R738 | 200.2 | 198.5 | | | 205.7 | 7.2 |
| R739 | 196.8 | 192.2 | | | 201.6 | 9.4 |

Table 6
Hardness and tensile properties of annealed and 1100 h aged Mo–47.5Re

| Test temperature (K) | Condition | Hardness ($kg/mm^2$) | Sample ID | YS (MPa) | UTS (MPa) | Uniform elongation (%) | Total elongation (%) | Reduction in area (%) |
|---|---|---|---|---|---|---|---|---|
| RT | Annealed | $334 \pm 2$ | R727 | 561 | 893 | 17.4 | 19.9 | – |
| | Aged 1098 K | $342 \pm 5$ | R731 | | | | | |
| | Aged 1248 K | $376 \pm 5$ | R735 | | | | | |
| | Aged 1398 K | $361 \pm 6$ | R739 | | | | | |
| 1073 | Annealed | | R728 | 270 | 510 | 15.3 | 25.0 | 83.9 |
| | Aged 1098 K | | R731 | 284 | 525 | 16.5 | 24.1 | – |
| | Aged 1098 K | | R732 | 278 | 513 | 16.3 | 28.2 | – |
| | Aged 1098 K | | R733 | 269 | 508 | 21.8 | 29.6 | 80.4 |
| 1223 | Annealed | | R754 | 300 | 464 | 15.1 | 29.6 | – |
| | Aged 1248 K | | R734 | 277 | 481 | 19.3 | 38.3 | 77.7 |
| | Aged 1248 K | | R735 | 262 | 442 | 15.4 | 36.1 | – |
| 1373 | Annealed | | R725 | 223 | 326 | 14.5 | 62.9 | 89.2 |
| | Aged 1398 K | | R737 | 275 | 367 | 8.8 | 34.8 | 69.8 |
| | Aged 1398 K | | R738 | 239 | 325 | 7.5 | 32.8 | – |

remnant σ particles from the annealed condition. Thus, no changes in tensile properties were measured for the 1098 K aged material over that of the as-annealed.

The further development of the χ phase in the 1248 K aged samples appears to have resulted in a measurable increase in hardness, though tensile strength remains unchanged relative to the annealed condition. Similar tensile curves were recorded for the as-annealed and 1248 K aged materials tested at 1223 K (Fig. 15(a)). Although the total elongation of the aged specimens is higher than that of the annealed material, presumably due to the decrease in solute concentration within the solid solution phase. Remarkably, both the as-annealed and aged samples tested at 1223 K exhibited similar yield strength to that of the as-annealed and 1098 K aged materials tested at 1073 K.

Following aging at 1398 K, substantial precipitation of the σ phase occurred along the boundaries of the solid solution grains. This resulted in increases in electrical resistivity and hardness over the as-annealed material. Although, the increase in hardness was not as great as that associated with the χ phase precipitated structure of the 1248 K aged material. The 1398 K aged material showed a small increase in tensile strength over the as-annealed material tested at 1373 K (Fig. 15(b)) consistent with the hardness results. While both the annealed and 1398 K aged specimens reach very high total elongations, the uniform elongation is only 14.5%, 8.8% and 7.5% for the annealed and two aged specimens, respectively. However, perhaps more important is the lack of work-hardening observed in both specimens. This loss of work-hardening may lead to premature localized necking dur-

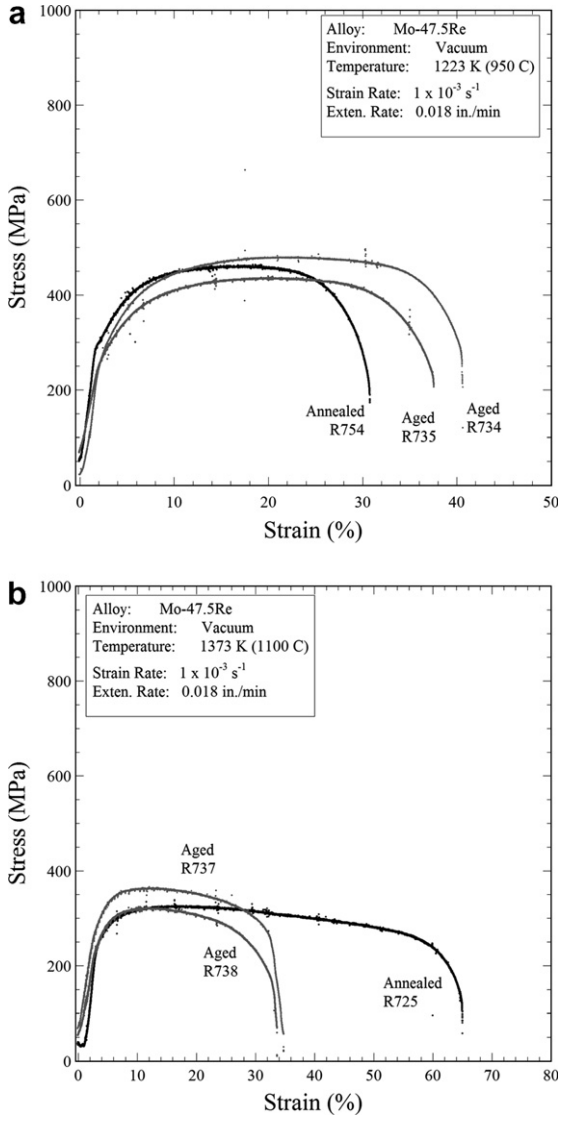


Fig. 15. Comparison of stress–strain curves for annealed and aged Mo–47.5Re. (a) 1248 K aged and as-annealed material tested at 1223 K, and (b) 1398 K aged and as-annealed material tested at 1373 K.

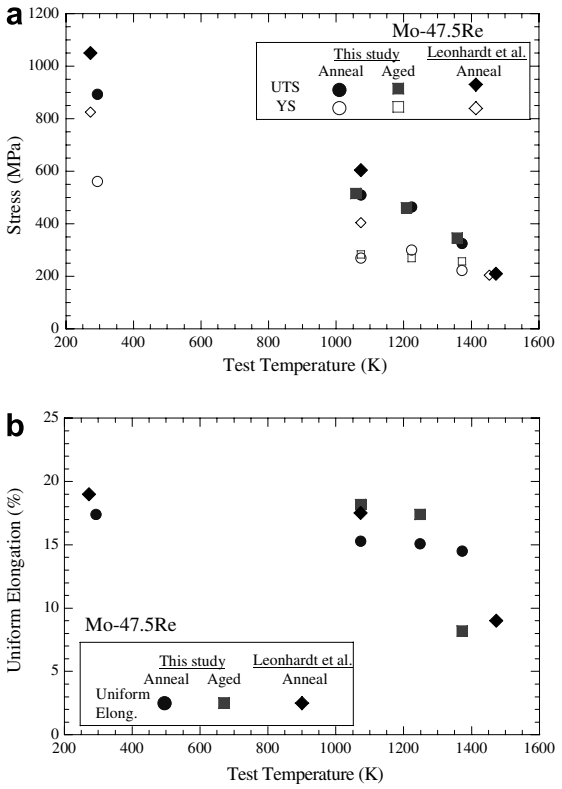


Fig. 16. Comparison of mechanical properties for annealed and aged Mo–47.5Re samples of this study with literature results [24].

ing service at high temperatures. The fracture surfaces of all as-annealed and aged Mo–47.5Re samples tested showed transgranular ductile failure occurring in the gage section.

The tensile properties of the aged and annealed Mo–47.5Re are plotted as a function of test temperature in Fig. 16 along with the data of Leonhardt et al. [24] for a powder metallurgy produced Mo–47.5Re alloy tested at similar temperatures. The measured values of UTS for this study are consistent with those of Leonhardt et al. At room temperature, the YS of the annealed alloy of this study is considerably lower than that for Leonhardt et al., however, this may be due to differences in processing treatment or σ phase distributions. The uniform elongations are also similar, considering that most values are from a single tensile test. Of particular interest is that the uniform elongation measured by Leonhardt et al. drops significantly between testing at 1073 and 1473 K, consistent with the observed loss of work-hardening in the samples of this study tested at 1373 K.

## 4. Conclusions

An evaluation of the microstructural changes resulting from 1100 h aging at 1098, 1248 and 1398 K was completed for Mo–41Re and Mo–47.5Re alloys, providing one of the first in depth analyses of the phases present, their distribution and affect on electrical resistivity and mechanical properties. Aging for 1100 h resulted in changes in electrical resistivity, hardness or tensile properties from the as-annealed condition for most of the

conditions investigated, indicating that some degree of microstructural evolution or solute redistribution had occurred during aging.

Changes in the hardness and electrical resistivity were measured for Mo–41Re aged at 1098 K over the as-annealed condition, but these effects diminished with increased aging temperature and may be related to the distribution of interstitials in the alloy. The lack of apparent change in tensile properties of Mo–41Re was due to the lack of change in the microstructure of alloy, with the material showing no evidence of precipitation at any of the aging conditions. Solute segregation of approximately 4 wt% Re at the grain boundaries was observed in both the as-annealed and aged conditions of the alloy.

The 1248 and 1398 K aged Mo–47.5Re alloy showed marked changes in electrical resistivity and tensile properties compared to the as-annealed condition, while no significant difference was observed for the 1098 K aged material. The changes in physical and mechanical properties of Mo–47.5Re were found to correlate with the observed changes in the microstructure of the alloy. The minor amount of $\chi$ phase precipitation following 1100 h of aging at 1098 K was not enough to produce a measurable change in properties over the as-annealed material. However, the development of the $\sigma$ phase along grain boundaries in Mo–47.5Re aged at 1398 K was found to be somewhat detrimental to mechanical properties, with the alloy exhibiting a reduction in uniform elongation. Although similar grain boundary precipitation was observed with the $\chi$ phase in the 1248 K aged material which did not show degraded mechanical properties, issues related to notch sensitivity, corrosion, and fatigue are not known. The evaluation of this alloy at longer aging times may lead to a further development of the grain boundary precipitates resulting in undesirable mechanical properties. This also includes the Mo–41Re, from which Re enrichment at the grain boundaries might lead to precipitation of $\sigma$ or $\chi$ phases at longer aging times or under radiation environments.

## Acknowledgements

The authors would like to thank J. Hack, R. Baranwal, T.M. Angeliu and Y. Ballout of the Naval Reactors Prime Contractor Team for many helpful technical discussions and guidance. The authors would like to thank Marie Williams, Mike Pershing and Cliff Davison for help in acid cleaning and annealing of the specimens prior to thermal aging; Jeffrey McNabb and Bob Sitterson for welding and leak testing the Alloy 600 aging cans; Brian Sparks and David Harper for thermal aging the encapsulated materials; Kathy Thomas and Jackie Mayotte for their help in preparing samples for microscopy. The authors would also like to thank E.K. Ohriner and E.P. George for their helpful discussions. This work was performed under the sponsorship of NASA's Project Prometheus and directed by DOE/NNSA Naval Reactors. Opinions and conclusions drawn by the authors are not endorsed by DOE/NNSA Naval Reactors. Research at the Oak Ridge National Laboratory SHaRE User Center was sponsored by the Division of Materials Sciences and Engineering, US Department of Energy. ORNL is managed for DOE by UT-Battelle, LLC, under contract DE-AC-05-00OR22725.

## References

[1] G.A. Geach, J.E. Hughes, in: F. Benesovsky (Ed.), Second Plansee Seminar, Pergamon, London, 1956.
[2] R.I. Jaffee, C.T. Sims, J.J. Harwood, in: F. Benesovsky (Ed.), Third Plansee Seminar, Springer-Verlag, Vienna, Austria, 1959.
[3] D.J. Maykuth, F.C. Holden, R.I. Jaffee, in: B.W. Gonser (Ed.), Electrochemical Society Symposium on Rhenium, Elsevier, New York, NY, 1962, p. 125.
[4] C.T. Sims, R.I. Jaffee, Trans. ASM 52 (1960) 929.
[5] J.G. Booth, R.I. Jaffee, E.I. Salkovitz, in: F. Benesovsky (Ed.), Fifth Plansee Seminar, Springer-Verlag, Vienna, Austria, 1959.
[6] A. Lawley, R. Maddin, Trans. TMS-AIME 224 (1962) 573.
[7] J.R. Stephens, W.R. Witzke, J. Less-Common Met. 29 (1972) 371.
[8] W.D. Klopp, J. Less-Common Met. 29 (1975) 261.
[9] D.L. Davidson, F.R. Brotzen, Acta Metall. 18 (1970) 463.
[10] A. Lawley, R. Maddin, Trans. Met. Soc. AIME 224 (1962) 573.
[11] A.D. Korotaev, A.N. Tyumentsev, V.V. Manako, Yu.P. Pinzhin, in: B.D. Bryskin (Ed.), Rhenium and Rhenium Alloys, TMS, Warrendale, PA, 1997, p. 671.
[12] P.L. Raffo, J. Less-Common Met. 17 (1969) 133.
[13] L.B. Lundberg, E.K. Ohriner, S.M. Tuominen, E.P. Whelan, Solution Softening in Molybdenum Rhenium Alloys, Physical Metallurgy and Technology of Molybdenum and its Alloys, AMAX, Greenwich, CT, 1985.
[14] W.D. Klopp, W.R. Witzke, NASA TM X-2576, 1972.
[15] J. Wadsworth, T.G. Nieh, J.J. Stephens, Scripta Metall. 20 (1986) 637.
[16] J. Wadsworth, T.G. Nieh, J.J. Stephens, Int. Met. Rev. 33 (1988) 131.
[17] E. Ohriner, ORNL, private communication, 2006.
[18] J.T. Busby, K.J. Leonard, L.L. Snead, F.W. Wiffen, S.J. Zinkle, J. Nucl. Mater., these Proceedings.
[19] Standard Test Method for Resistivity of Electrical Conductor Materials, ASTM Designation B 193-87. ASTM Stan-

dards Online, American Society for Testing and Materials, Philadelphia, PA, 1992.
[20] A. Buch, Pure Metal Properties: A Scientific Technical Handbook, ASM International and Freund Publishing House Ltd., Materials Park, OH, 1999.
[21] Standard Test Method for Tension Testing of Metallic Materials, ASTM standard E8-04, ASTM Standards Online, American Society for Testing and Materials, Philadelphia, PA, 2001.
[22] Y. Nemoto, A. Hasegawa, M. Satou, K. Abe, Y. Hiraoka, J. Nucl. Mater. 324 (2004) 62.
[23] K. Schroeder, CRC Handbook of Electrical Resistivities of Binary Metallic Alloys, CRC Press, Boca Raton, FL, 1983.
[24] T. Leonhardt, J. Carlen, M. Buck, R. Weiju, C. Stevens, in: M.S. El-Genk (Ed.), Space Technology and Applications International Forum–STAIF 1999, American Institute of Physics 458 (10) (1999) 685.
[25] T.B. Massalski (Ed.), Binary Alloy Phase Diagrams, vol. 2, ASM International, Metals Park, OH, 1986.
[26] J.C. Carlen, B.D. Bryskin, J. Mater. Eng. Perform. 32 (2) (1994) 282.
[27] J.A. Shields, in: M.S. El-Genk (Ed.), Space Technology and Applications International Forum-STAIF 2005, American Institute of Physics, 2005, p. 835.
[28] R.A. Erck, L.E. Rehn, Philos. Mag. A 62 (1) (1990) 29.
[29] K. Ogawa, R. Maddin, Acta Met. 12 (1964) 1161.
[30] R.L. Mannheim, J.L. Garin, J. Mater. Process. Technol. 143&144 (2003) 533.
[31] D.J. Senor, J.A. Horak, Material Property Correlations for W-25Re, Mo–50Re and ASTAR-811C, Oak Ridge National Laboratory unpublished report, 1989, p. 1.